IFSM-76-74

FC.

LEHIGH UNIVERSITY

STRESS SINGULARITY FOR A CRACK WITH AN ARBITRARILY CURVED FRONT

BY

R. J. HARTRANFT
G. C. SIH

TECHNICAL REPORT
APRIL 1976

DEPARTMENT OF THE NAVY
OFFICE OF NAVAL RESEARCH
ARLINGTON, VIRGINIA 22217

STRESS SINGULARITY FOR A CRACK WITH AN ARBITRARILY CURVED FRONT

by

R. J. Hartranft

G. C. Sih

LEHIGH UNIVERSITY
Institute of Fracture and Solid Mechanics
Bethlehem, Pennsylvania 18015

April 1976

Technical Report

Prepared under Contract N00014-76-C-0094

for

Department of the Navy

Office of Naval Research

Arlington, Virginia 22217

ABSTRACT

To investigate the possibility of a point of a crack front propagating in a direction not in the normal plane of the crack front, the three-dimensional form of the crack front stress field is obtained. To simplify comparisons of the states of stress at various points lying on a spherical surface centered at a point of the crack front, a local spherical coordinate system is used. It is found that the crack propagation will be from each point of the crack front in a direction lying in the normal plane.

The results are used in conjunction with the strain energy density fracture criterion for the problem of an elliptical crack. The plane of the flat elliptical crack makes an arbitrary angle with the field of uniform applied tensile stress. Crack growth directions for various positions along the crack front are determined, and loads required for fracture for various angles are obtained.

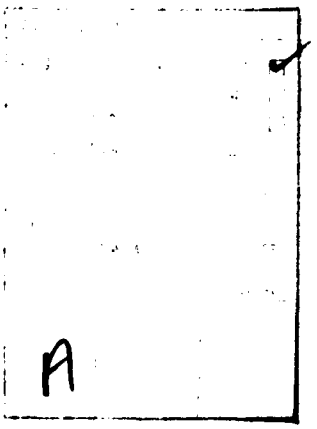

INTRODUCTION

Cracks of particular shapes have been considered by several authors. The plane strain geometry and loading always result in the familiar plane strain crack tip stress singularity established by Williams [1]. Similarly, the plane strain geometry subjected to anti-plane loading always leads to the form of crack tip stress singularity given in [2]. These forms will be referred to as the two-dimensional results. They contain the three stress intensity factors, k_1, k_2, and k_3. Examination of the two-dimensional results shows that the singular part of the crack tip stresses depends explicitly on position relative to the crack, and implicitly on the other parameters (load, geometry, material) through the stress intensity factors.

This same type of two-dimensional geometry subjected to arbitrary three-dimensional loading was the subject of an eigenfunction expansion investigation [3]. It was found that the crack tip stress singularity was identical in form to the two-dimensional results, with the exception that the stress intensity factors depend, in general, on the position of the point of the crack front nearest the point at which the stresses are computed.

Irwin [4] showed that the form taken by the stress field in [5] for a penny shaped crack is also the same as the two-dimensional result. Progress since then has established that

this is true for very general loads. For a review of the problem of the penny shaped crack, see [6], which contains a large number of stress intensity factors evaluated for various loads.

Finally, for the cases considered, the form of the stress field near the edge of an elliptical crack is also given by the two-dimensional results [7]. Reference [6] contains several examples of loading and the corresponding stress intensity factors.

Although not proved, it seems quite likely that similar results apply to arbitrary cracks. The starting point in this investigation is the assumption that the two-dimensional results give the form of the stress singularity for an arbitrary crack. The crack front is a general curve in space, described implicitly by its curvature and torsion. It will also be assumed that the osculating plane of the crack front curve is tangent to the free surfaces of the crack at each point.

A geometrical analysis provides the stress field referred to local spherical coordinates. The strain energy density theory [8] when applied in three-dimensions [9] requires this result so that minimums of strain energy density on spherical surfaces can be located. The result is surprisingly simple when the appropriate choice of coordinate system is made. A different choice of coordinates can lead to results as complicated as those in Appendix I [6,9].

The results are applied to mixed mode loading of a flat elliptical crack. The stress intensity factors of [7] can be combined to give the crack front stress singularity for a field of uniform tension at an arbitrary angle to the plane of the crack. The various crack growth directions and loads are displayed in Appendix II as functions of the parameters involved.

A future application of this result to the transverse crack in a thick plate is anticipated. The development of a shear lip due to the interaction of a curved (thumbnail) crack front with the free surface will lead to mixed mode crack front stress fields. The analysis of additional crack growth under mixed mode loading requires further work on the finite element numerical stress analysis. But when this is obtained, the strain energy density fracture criterion will be available for direct application.

Further work to include higher order terms seems appropriate for use in developing special crack front elements in finite element formulations of problems involving curved cracks. It is expected that the curvature and torsion of the curve and their derivatives along the crack will be required. Derivatives of the stress intensity factors may also appear in the result.

LOCAL STRESS FIELD

Let P be a point of the curve defining the crack front and let $\underline{n}$, $\underline{b}$, and $\underline{t}$ be the normal, binormal, and tangent (unit) vectors at P. The plane defined by the normal and tangent, known as the osculating plane, will be assumed to coincide with the tangent to the free surfaces of the crack at P. This is by no means necessary, but for a naturally growing crack, it seems reasonable. For an element in the normal plane, defined by $\underline{n}$ and $\underline{b}$, as shown in Figure 1, the appropriate form of the stress field is the two-dimensional result,

$$\sigma_n = \frac{k_1}{\sqrt{2r}} \cos\frac{\theta}{2}\left[1 - \sin\frac{\theta}{2}\sin\frac{3\theta}{2}\right] - \frac{k_2}{\sqrt{2r}} \sin\frac{\theta}{2}\left[2 + \cos\frac{\theta}{2}\cos\frac{3\theta}{2}\right]$$

$$\sigma_b = \frac{k_1}{\sqrt{2r}} \cos\frac{\theta}{2}\left[1 + \sin\frac{\theta}{2}\sin\frac{3\theta}{2}\right] + \frac{k_2}{\sqrt{2r}} \sin\frac{\theta}{2}\cos\frac{\theta}{2}\cos\frac{3\theta}{2}$$

$$\sigma_t = 2\nu\left[\frac{k_1}{\sqrt{2r}} \cos\frac{\theta}{2} - \frac{k_2}{\sqrt{2r}} \sin\frac{\theta}{2}\right]$$

$$\tau_{nb} = \frac{k_1}{\sqrt{2r}} \sin\frac{\theta}{2}\cos\frac{\theta}{2}\cos\frac{3\theta}{2} + \frac{k_2}{\sqrt{2r}} \cos\frac{\theta}{2}\left[1 - \sin\frac{\theta}{2}\sin\frac{3\theta}{2}\right]$$

$$\tau_{nt} = -\frac{k_3}{\sqrt{2r}} \sin\frac{\theta}{2}$$

$$\tau_{bt} = \frac{k_3}{\sqrt{2r}} \cos\frac{\theta}{2} \qquad (1)$$

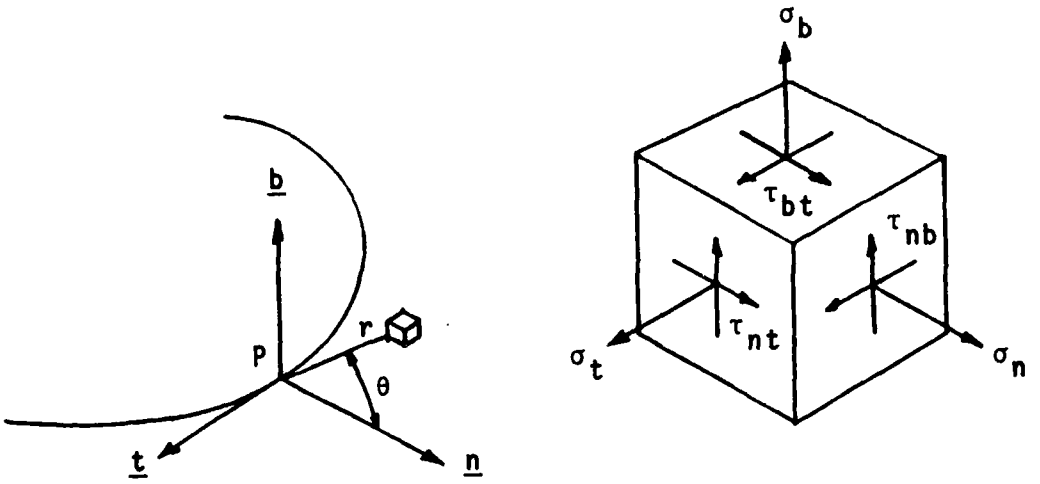

Figure 1: Crack front stresses in the normal plane.

These stresses act on an element with edges in the $\underline{n}$, $\underline{b}$, and $\underline{t}$ directions. The stresses on the plane, $\theta=0$ reduce to

$$\sigma_b = \frac{k_1}{\sqrt{2r}}, \quad \tau_{nb} = \frac{k_2}{\sqrt{2r}}, \quad \tau_{bt} = \frac{k_3}{\sqrt{2r}} \qquad (2)$$

In all cases, k_1, k_2, and k_3 are to be evaluated at point P of the crack front. The expressions for the stresses omit terms of $O(1)$, which are finite at the crack front.

GEOMETRY

Consider two points, P_o and P, on the crack front as shown in Figure 2. Regard P_o as fixed and P as moving. Then

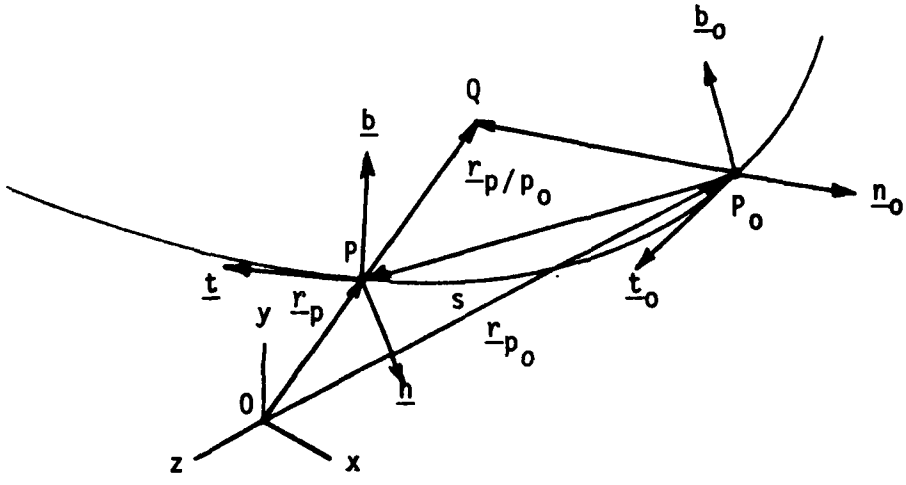

Figure 2: Vector triads at two points.

the position of P, $\underline{r}_P$, and the unit vectors, $\underline{n}$, $\underline{b}$, and $\underline{t}$ may be regarded as functions of the arc length, s, from P_o to P. It is shown in differential geometry [10] that

$$\frac{d\underline{r}_P}{ds} = \underline{t} \qquad \frac{d\underline{n}}{ds} = \kappa\underline{t} + \tau\underline{b}$$

$$\frac{d\underline{b}}{ds} = -\tau\underline{n} \qquad \frac{d\underline{t}}{ds} = -\kappa\underline{n} \tag{3}$$

The sign of the curvature, κ, is opposite that in [10] because $\underline{n}$ here points to the convex side of the curve when κ is positive. When the torsion, τ, is positive, $\underline{n}$ and $\underline{b}$ turn in the direction of a right-handed screw about $\underline{t}$ as P moves in the

direction of $\underline{t}$.

If s is small, Taylor series expansions of the vectors about s=0 are

$$\underline{n} = \underline{n}_o + \left.\frac{d\underline{n}}{ds}\right|_{P_o} s + O(s^2) = \underline{n}_o + (\kappa_o \underline{t}_o + \tau_o \underline{b}_o)s + O(s^2)$$

$$\underline{b} = \underline{b}_o + \left.\frac{d\underline{b}}{ds}\right|_{P_o} s + O(s^2) = \underline{b}_o - \tau_o \underline{n}_o s + O(s^2) \qquad (4)$$

$$\underline{t} = \underline{t}_o + \left.\frac{d\underline{t}}{ds}\right|_{P_o} s + O(s^2) = \underline{t}_o - \kappa_o \underline{n}_o s + O(s^2)$$

$$\underline{r}_P = \underline{r}_{P_o} + \left.\frac{d\underline{r}_P}{ds}\right|_{P_o} s + O(s^2) = \underline{r}_{P_o} + \underline{t}_o s + O(s^2)$$

where equations (3) have been used. The zero subscript indicates that the term is evaluated at P_o.

The position of an arbitrary point Q may be expressed in two ways. In terms of its coordinates, n_o, b_o, and t_o, in the reference frame at P_o,

$$\underline{r}_Q = \underline{r}_{P_o} + n_o \underline{n}_o + b_o \underline{b}_o + t_o \underline{t}_o \qquad (5)$$

Using the coordinates, n, b, and t, in the reference frame at P,

$$\underline{r}_Q = \underline{r}_P + n\underline{n} + b\underline{b} + t\underline{t} \qquad (6)$$

Equating (5) and (6) and using equations (4) the relation between the two sets of coordinates is found to be

$$n_o = n - (\kappa_o t + \tau_o b)s + O(s^2)$$

$$b_o = b + \tau_o n s + O(s^2) \qquad (7)$$

$$t_o = t + (1 + \kappa_o n)s + O(s^2)$$

The direction cosines needed for transforming the stress components from one reference frame to the other may be expressed as in Table I. The elements in the table are cosines

Table I: Direction cosines of the transformation

	$\underline{n}_o$	$\underline{b}_o$	$\underline{t}_o$
$\underline{n}$	1	$\tau_o s$	$\kappa_o s$
$\underline{b}$	$-\tau_o s$	1	0
$\underline{t}$	$-\kappa_o s$	0	1

of the angles between the two sets of unit vectors. These are easily obtained from equations (4). Note that terms of $O(s^2)$ have been omitted from Table I.

TRANSFORMATION OF COORDINATES

Suppose the point Q of Figure 2 is the location of the elements shown in Figures 1 and 3. From Figures 1 and 3, the coordinates of Q, which are related by equations (7), may be

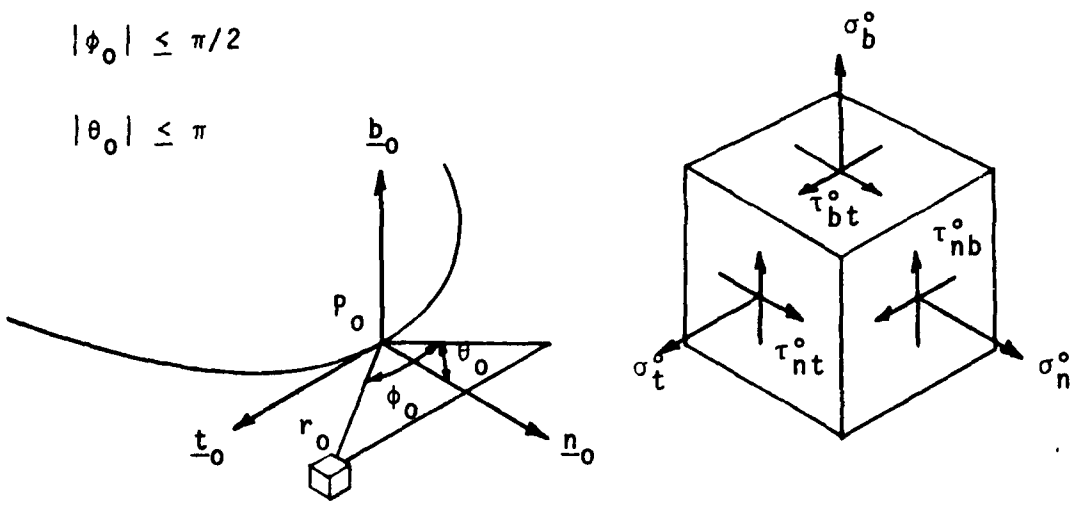

Figure 3: Crack front stresses in an arbitrary position.

written as

$$\begin{aligned} n &= r\cos\theta & n_o &= r_o \cos\phi_o \cos\theta_o \\ b &= r\sin\theta & b_o &= r_o \cos\phi_o \sin\theta_o \\ t &= 0 & t_o &= r_o \sin\phi_o \end{aligned} \tag{8}$$

Then equations (7) become

$$r_o \cos\phi_o \cos\theta_o = r\cos\theta - \tau_o r \sin\theta\, s + O(s^2)$$

$$r_o \cos\phi_o \sin\theta_o = r\sin\theta + \tau_o r \cos\theta\, s + O(s^2) \qquad (9)$$

$$r_o \sin\phi_o = (1 + \kappa_o r\cos\theta)s + O(s^2)$$

For the present investigation, P_o and the spherical coordinates, r_o, θ_o, and ϕ_o, are regarded as given. Equations (9) are then used to determine r, θ, and s. That is, the position of the point P such that Q lies in the normal plane at P is to be determined. The first two of equations (9) give

$$r\sin\theta = r_o \cos\phi_o [\sin\theta_o - \tau_o \cos\theta_o\, s] + O(s^2)$$

$$r\cos\theta = r_o \cos\phi_o [\cos\theta_o + \tau_o \sin\theta_o\, s] + O(s^2) \qquad (10)$$

and the third becomes

$$r_o \sin\phi_o = (1 + \kappa_o r_o \cos\phi_o \cos\theta_o)s + O(s^2) \qquad (11)$$

Equation (11) has the solution

$$s = r_o \sin\phi_o + O(r_o^2) \qquad (12)$$

and equations (10) become

$$r \sin\theta = r_o \cos\phi_o \sin\theta_o + O(r_o^2)$$

$$r \cos\theta = r_o \cos\phi_o \cos\theta_o + O(r_o^2) \tag{13}$$

In view of equations (13), the coordinates r and θ are

$$r = r_o \cos\phi_o + O(r_o^2)$$

$$\theta = \theta_o + O(r_o) \tag{14}$$

From these, one obtains such results as

$$\frac{1}{\sqrt{2r}} = \frac{1}{\sqrt{2r_o}\cos\phi_o}\,[1 + O(r_o)]$$

$$\sin\theta = \sin\theta_o + O(r_o),\quad \cos\theta = \cos\theta_o + O(r_o) \tag{15}$$

for use in equations (1).

TRANSFORMATION OF STRESS

The two sets of stress components shown in Figures 1 and 3 both describe the state of stress at the same point Q. Thus they are related by the standard transformation formulas for stress. For example,

$$\sigma_n^o = \ell_{nn}^2\sigma_n + \ell_{nb}^2\sigma_b + \ell_{nt}^2\sigma_t + 2\ell_{nn}\ell_{nb}\tau_{nb}$$

$$+ 2\ell_{nn}\ell_{nt}\tau_{nt} + 2\ell_{nb}\ell_{nt}\tau_{bt}$$

$$\tau_{nb}^o = \ell_{nn}\ell_{bn}\sigma_n + \ell_{nb}\ell_{bb}\sigma_b + \ell_{nt}\ell_{bt}\sigma_t \tag{16}$$

$$+ 2\ell_{nn}\ell_{bb}\tau_{nb} + 2\ell_{nn}\ell_{bt}\tau_{nt} + 2\ell_{nb}\ell_{bt}\tau_{bt}$$

where $\ell_{ab} = \underline{a}_o \cdot \underline{b}$ is the cosine of the angle between the $\underline{a}_o$ direction and the $\underline{b}$ direction. These are shown in Table I, where the first subscript on ℓ_{ab} indicates the proper column and the second, the row.

The result for σ_n^o is given to show the order of approximation involved in the stress transformation due to neglecting terms in the direction cosines.

$$\sigma_n^o = \sigma_n - 2(\kappa_o\tau_{nt} + \tau_o\tau_{nb})s + O(s^2) \tag{17}$$

Similar results can be written for the other stress components, but since s is given by equation (12), the linear terms in s are of the same order of magnitude as the terms neglected in equations (1). Therefore, to the order of accuracy required,

$$\sigma_n^o = \sigma_n + O(s) \quad \tau_{nb}^o = \tau_{nb} + O(s)$$

$$\sigma_b^o = \sigma_b + O(s) \quad \tau_{nt}^o = \tau_{nt} + O(s) \tag{18}$$

$$\sigma_t^o = \sigma_t + O(s) \quad \tau_{bt}^o = \tau_{bt} + O(s)$$

LOCAL STRESS FIELD IN SPHERICAL COORDINATES

The stress components in Figure 3 can be evaluated after one additional consideration. The stress intensity factors in equations (1) are to be evaluated at point P. However, Taylor series expansions can be used to relate these values to the values at point P_o. Thus,

$$\begin{aligned} k_1 &= k_1^o + 0(s) \\ k_2 &= k_2^o + 0(s) \\ k_3 &= k_3^o + 0(s) \end{aligned} \tag{19}$$

By assembling together equations (1), (12), (14), (15), (18), and (19), the desired result is obtained.

$$\sigma_n^o = \frac{k_1^o}{\sqrt{2r_o\cos\phi_o}} \cos\frac{\theta_o}{2}\left[1 - \sin\frac{\theta_o}{2}\sin\frac{3\theta_o}{2}\right]$$

$$- \frac{k_2^o}{\sqrt{2r_o\cos\phi_o}} \sin\frac{\theta_o}{2}\left[2 + \cos\frac{\theta_o}{2}\cos\frac{3\theta_o}{2}\right]$$

$$\sigma_b^o = \frac{k_1^o}{\sqrt{2r_o\cos\phi_o}} \cos\frac{\theta_o}{2}\left[1 + \sin\frac{\theta_o}{2}\sin\frac{3\theta_o}{2}\right]$$

$$+ \frac{k_2^o}{\sqrt{2r_o\cos\phi_o}} \sin\frac{\theta_o}{2}\cos\frac{\theta_o}{2}\cos\frac{3\theta_o}{2}$$

$$\sigma_t^o = 2\nu \left[\frac{k_1^o}{\sqrt{2r_o\cos\phi_o}} \cos\frac{\theta_o}{2} - \frac{k_2^o}{\sqrt{2r_o\cos\phi_o}} \sin\frac{\theta_o}{2}\right]$$

$$\tau_{nb}^o = \frac{k_1^o}{\sqrt{2r_o\cos\phi_o}} \sin\frac{\theta_o}{2} \cos\frac{\theta_o}{2} \cos\frac{3\theta_o}{2}$$

$$+ \frac{k_2^o}{\sqrt{2r_o\cos\phi_o}} \cos\frac{\theta_o}{2} \left[1 - \sin\frac{\theta_o}{2} \sin\frac{3\theta_o}{2}\right] \qquad (20)$$

$$\tau_{nt}^o = - \frac{k_3^o}{\sqrt{2r_o\cos\phi_o}} \sin\frac{\theta_o}{2}$$

$$\tau_{bt}^o = \frac{k_3^o}{\sqrt{2r_o\cos\phi_o}} \cos\frac{\theta_o}{2}$$

In equations (20), terms which remain finite as $r_o \to 0$ are omitted.

Thus, the spherical coordinates of Figure 3 result in a simple form for the crack front stress singularity. It should be noted that, to the order of approximation used, the stresses on the element of Figure 3 are the same as those on an element in the normal ($\underline{n}_o\underline{b}_o$) plane located a distance $r_o \cos\phi_o$ from P_o and an angle θ_o from $\underline{n}_o$. The more complicated form resulting from the choice of coordinates used in [6,9] is given in Appendix I.

STRAIN ENERGY DENSITY

For plane problems, the strain energy density fracture criterion [8] states that crack growth is toward the point

on a circle centered at the crack tip which has the smallest strain energy density. Furthermore, the growth begins when this smallest value of the strain energy density reaches the allowable value for the material.

A similar criterion has been stated [9] for three-dimensional problems. Each point of the crack front must be considered separately. A small sphere, centered at a particular point of the crack front, is used to replace the circle in the two-dimensional case. The criterion states that crack growth is directed along the line from the center of the sphere to the point on the sphere with the smallest strain energy density. The collection of these lines, one for each point of the crack front, defines the new crack surface. Growth along these directions begins when the value of minimum strain energy density reaches the maximum which the material will tolerate.

In use, since some points fail before others, it is convenient to imagine an increment of crack growth proportional in length to the value of minimum strain energy density at each point. Thus, the points failing first have more new crack surface adjacent to them. The usual warning [11,12] that the calculations apply only to the first crack growth from the initial geometry is appropriate. For very brittle materials, it has been noted [11] that predictions based on the initial crack geometry agree well with experiment for large amounts of crack growth.

Since the form of equations (20) is so much like the two-dimensional result, much use can be made of [8]. The strain energy density can, in fact, be written easily as

$$\frac{dW}{dV} = \frac{S}{r_o \cos\phi_o} + O(1) \tag{21}$$

where

$$S = a_{11}(k_1^o)^2 + 2a_{12}k_1^o k_2^o + a_{22}(k_2^o)^2 + a_{33}(k_3^o)^2 \tag{22}$$

The coefficients in equation (22) are exactly the same as in [8].

$$\begin{aligned} 16\,Ga_{11} &= (3 - 4\nu - \cos\theta_o)(1 + \cos\theta_o) \\ 16\,Ga_{12} &= 2\sin\theta_o\,(\cos\theta_o - 1 + 2\nu) \\ 16\,Ga_{22} &= 4(1-\nu)(1 - \cos\theta_o) + (3\cos\theta_o - 1)(1 + \cos\theta_o) \\ 16\,Ga_{33} &= 4 \end{aligned} \tag{23}$$

where G and ν are the shear modulus and Poisson's ratio, respectively.

When dependence on the angle ϕ_o is analyzed, it is seen that the minimum of equation (21) occurs in the normal plane,

$$\phi_o^* = 0 \tag{24}$$

The remainder of the analysis is similar in some ways to that in [8]. Given the stress intensity factors, one computes the angle, θ_o^* which minimizes equation (22). The minimum value is denoted by S^*. Then crack growth occurs when

$$S^* = S_{cr} = \frac{1-2\nu}{4G} k_{Ic}^2 \tag{25}$$

in the direction defined by $\phi_o = \phi_o^* = 0$ and $\theta_o = \theta_o^*$. The plane strain fracture toughness denoted here by k_{Ic} is equal to that defined by ASTM divided by $\sqrt{\pi}$.

The results differ from two-dimensional analyses by virtue of the fact that the stress intensity factors, in general, vary from point to point along the crack front. Thus, the new crack surface is generally a warped surface of the type shown in [6,9].

The problem of uniform tension of an embedded elliptical crack is presented as an example in Appendix II. This problem has been discussed in [6,9], but Appendix II contains several results correcting the details of [6,9].

APPENDIX I

Suppose the point Q at which the stresses of Figure 3 are to be determined is located by the spherical coordinates shown in Figure 4. The ranges of the angles θ_1, ϕ_1 are not the con-

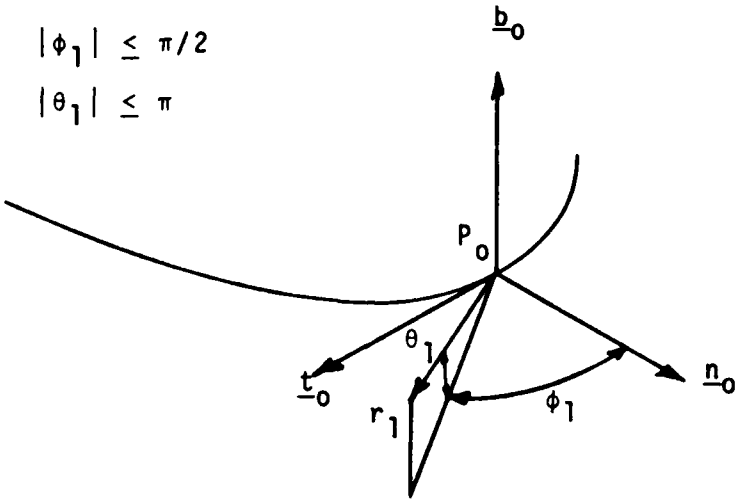

Figure 4: Alternative spherical coordinates.

ventional ones, but are chosen so that in the normal ($\underline{n}_o\underline{b}_o$) plane the two-dimensional form of the stress singularity is recovered.

In the transformation of coordinates, equations (8) are replaced by

$$n_o = r_1 \cos\theta_1 \cos\phi_1$$

$$b_o = r_1 \sin\theta_1 \qquad (26)$$

$$t_o = r_1 \cos\theta_1 \sin\phi_1$$

Then it is found that

$$s = r_1 \cos\theta_1 \sin\phi_1 + O(r_1^2)$$

$$r \sin\theta = r_1 \sin\theta_1 + O(r_1^2) \qquad (27)$$

$$r \cos\theta = r_1 \cos\theta_1 \cos\phi_1 + O(r_1^2)$$

Therefore,

$$\tan\theta = \frac{\tan\theta_1}{\lambda}$$

$$r = r_1 \lambda\kappa \cos\theta_1 \qquad (28)^*$$

where

$$\lambda = \cos\phi_1$$

$$\kappa = \mathrm{sgn}(\cos\theta_1) \sqrt{1 + \left(\frac{\tan\theta_1}{\lambda}\right)^2} \qquad (29)^{**}$$

The definition of λ in equations (29) differs from that in [6,9] because of an error in determining the relationship between the elliptical coordinates and the spherical coordinates

---

* The terms omitted in this and subsequent equations are all one order of magnitude smaller than the last term written.

** The symbol for curvature is also used here to make comparisons with [6,9] easier. There should be no confusion because curvature is contained nowhere in Appendix I.

near the crack front. Equation (29) is the correct form to use.

Equations (28) and (29) allow one to compute the terms required in equations (1). Thus, one has

$$\tan\theta = \mathrm{sgn}(\tan\theta_1)\sqrt{\kappa^2-1}$$

$$\sin\theta = \mathrm{sgn}(\tan\theta_1)\frac{1}{\kappa}\sqrt{\kappa^2-1}$$

$$\cos\theta = \frac{1}{\kappa}$$

$$\sin\frac{\theta}{2} = \mathrm{sgn}(\sin\theta_1)\sqrt{\frac{\kappa-1}{2\kappa}}$$

$$\cos\frac{\theta}{2} = \sqrt{\frac{\kappa+1}{2\kappa}} \qquad (30)$$

$$\sin\frac{3\theta}{2} = \mathrm{sgn}(\sin\theta_1)\frac{2+\kappa}{\kappa}\sqrt{\frac{\kappa-1}{2\kappa}}$$

$$\cos\frac{3\theta}{2} = \frac{2-\kappa}{\kappa}\sqrt{\frac{\kappa+1}{2\kappa}}$$

$$\frac{1}{\sqrt{2r}}\sin\frac{\theta}{2} = \frac{1}{\sqrt{2r_1}}\frac{\mathrm{sgn}(\sin\theta_1)}{|\kappa|}\sqrt{\frac{\kappa-1}{2\lambda\cos\theta_1}}$$

$$\frac{1}{\sqrt{2r}}\cos\frac{\theta}{2} = \frac{1}{\sqrt{2r_1}}\frac{1}{|\kappa|}\sqrt{\frac{\kappa+1}{2\lambda\cos\theta_1}}$$

The stress field obtained by substituting equations (30) into equations (1) and using equations (18), (19), and (27) is

$$\sigma_n^o = \frac{k_1^o}{\sqrt{2r_1}}(\kappa^2 - \kappa + 2)A - \frac{k_2^o}{\sqrt{2r_1}}(3\kappa^2 + \kappa + 2)B$$

$$\sigma_b^o = \frac{k_1^o}{\sqrt{2r_1}}(3\kappa^2 + \kappa - 2)A - \frac{k_2^o}{\sqrt{2r_1}}(\kappa^2 - \kappa - 2)B$$

$$\sigma_t^o = 2\nu\left[\frac{k_1^o}{\sqrt{2r_1}}2\kappa^2 A - \frac{k_2^o}{\sqrt{2r_1}}2\kappa^2 B\right] \qquad (31)$$

$$\tau_{nb}^o = -\frac{k_1^o}{\sqrt{2r_1}}(\kappa^2 - \kappa - 2)B + \frac{k_2^o}{\sqrt{2r_1}}(\kappa^2 - \kappa + 2)A$$

$$\tau_{nt}^o = -\frac{k_3^o}{\sqrt{2r_1}}2\kappa^2 B$$

$$\tau_{bt}^o = \frac{k_3^o}{\sqrt{2r_1}}2\kappa^2 A$$

where

$$A = \frac{1}{2|\kappa|^3}\sqrt{\frac{\kappa+1}{2\lambda\cos\theta_1}},\quad B = \frac{\mathrm{sgn}(\sin\theta_1)}{2|\kappa|^3}\sqrt{\frac{\kappa-1}{2\lambda\cos\theta_1}} \qquad (32)$$

Except for the correction of λ (equation (29)) and a more precise treatment of signs, equations (31) agree with those of [6,9].

The complicated form of equations (31) makes it difficult to find, except by numerical analysis, that the minimum strain energy density occurs when $\phi_1 = 0$. The form of equations (20) makes the result obvious.

APPENDIX II: ELLIPTICAL CRACK

The mixed mode loading of an infinite elastic body containing a flat elliptical crack is accomplished as in Figure 5 by inserting the crack at an angle to the direction of a

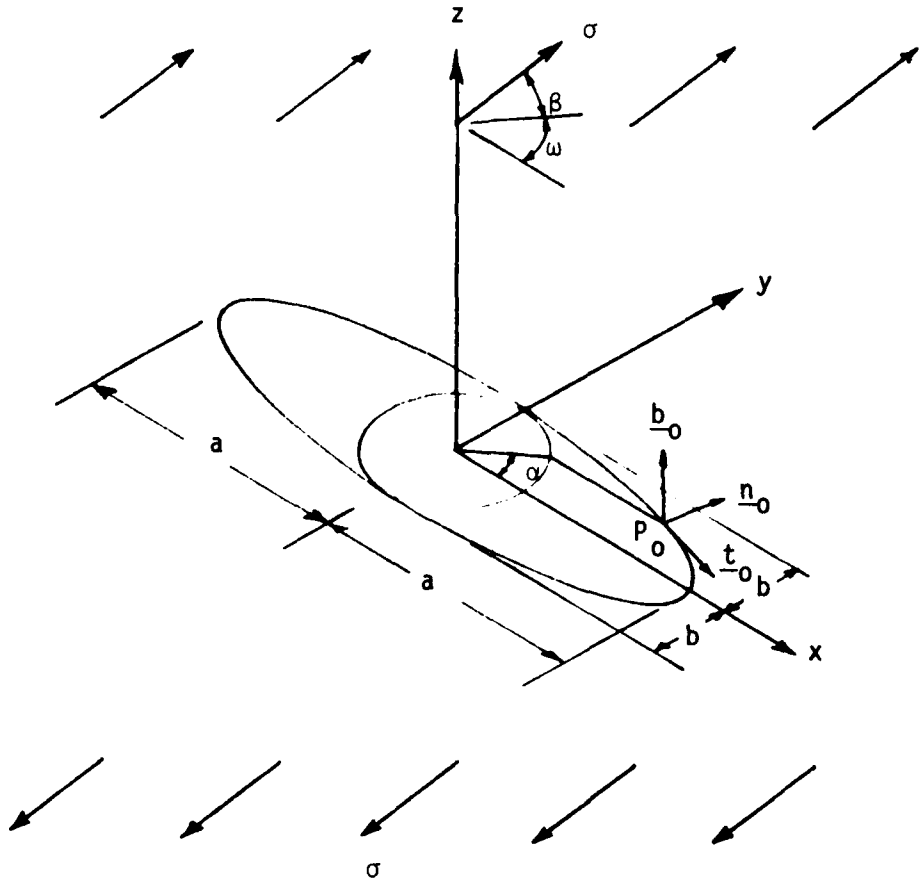

Figure 5: Elliptical crack at an angle to a field of uniform tension in an infinite material.

field of uniform tension. The coordinates of point P_o on the ellipse are given in terms of the parametric angle, α, by

$$x = a\cos\alpha,\quad y = b\sin\alpha \tag{33}$$

The stress intensity factors at point P_o [7] are

$$k_1^o = \frac{\sigma\sqrt{a_e}}{E(k)}\sin^2\beta$$

$$k_2^o = \sigma\sqrt{a_e}k'k^2\frac{a}{a_e}\sin\beta\cos\beta\left[\frac{\sin\alpha\sin\omega}{(k^2+\nu k'^2)E(k)-\nu k'^2K(k)}\right.$$

$$\left.+\frac{k'\cos\alpha\cos\omega}{(k^2-\nu)E(k)+\nu k'^2K(k)}\right] \tag{34}$$

$$k_3^o = (1-\nu)\,\sigma\sqrt{a_e}k'k^2\frac{a}{a_e}\sin\beta\cos\beta\left[-\frac{k'\cos\alpha\sin\omega}{(k^2+\nu k'^2)E(k)-\nu k'^2K(k)}\right.$$

$$\left.+\frac{\sin\alpha\cos\omega}{(k^2-\nu)E(k)+\nu k'^2K(k)}\right]$$

where $a_e = b\sqrt{1-k^2\cos^2\alpha}$

$$k' = \frac{b}{a} \qquad k = \sqrt{1-\frac{b^2}{a^2}}$$

and K(k) and E(k) are complete elliptic integrals of the first and second kinds, respectively.

These stress intensity factors can be substituted into equation (22), and the fracture angle θ_o^* determined for various angles of loading, β and ω, crack diameter ratios, b/a, and positions on the crack front, α. The point of the crack

front with the largest value of the minimum S^* will control the load required to cause failure, σ_{cr}. The value of this critical applied stress is obtained from equation (25).

Several results in [9] are modified by these calculations. Table 9-1* is no longer applicable since the minimum value of energy density occurs in the normal plane**. Table 1, containing corrected values of Table 9-2, shows the direction of minimum strain energy density corresponding to tensile loading for various points along the crack front. Also given are the normalized minimum values of the strain energy density and its distortional (S_d) and dilatational (S_v) parts. Corrected values for Table 9-3 are given in Table 2. Since the correct values of the minima, S^*, are larger than those reported in [9], the failure loads will be smaller than in [9].

Figure 6 shows the direction of crack growth at various points of the crack front (specified by α) for b/a = 0.5. The loads are applied symmetrically with respect to the xz-plane. As a result, the ends of the minor axis ($\alpha = 90°$) are undergoing Mode I and III deformation only, and the crack grows straight ahead under tension. Other values of the fracture angle are given as functions of the angle of inclination of

---

* The labels, Table 9-1, Figure 9-1, etc., will be used to designate Table 1, Figure 1, etc., in reference [9]. Labels without the 9-prefix refer to tables and figures in this Report.

** In the notation of [9], $\phi_0 = 0$.

Table 1. Fracture angles, θ_o^*, and S^* for b/a = 0.5, ν = 0.33, ω=0, and β = 60°. (Tensile loading)

α	θ_o^*	$16GS^*/\sigma^2 b$	$16GS_d^*/\sigma^2 b$	$16GS_v^*/\sigma^2 b$
0	-47.55°	0.4613	0.1208	0.3405
15°	-44.85°	0.5015	0.1535	0.3480
30°	-38.50°	0.5991	0.2291	0.3701
45°	-30.58°	0.7144	0.3144	0.3999
60°	-21.56°	0.8171	0.3890	0.4280
75°	-11.29°	0.8870	0.4394	0.4476
90°	0	0.9118	0.4572	0.4545

Table 2. Fracture angles, θ_o^*, and S^* for b/a = 0.5, ν = 0.33, ω=0, and β = 60°. (Compressive loading)

α	θ_o^*	$16GS^*/\sigma^2 b$	$16GS_d^*/\sigma^2 b$	$16GS_v^*/\sigma^2 b$
0	124.78°	0.0884	0.0778	0.01056
15°	128.24°	0.1168	0.1095	0.00730
30°	136.47°	0.1851	0.1823	0.00272
45°	146.56°	0.2648	0.2643	0.00059
60°	157.35°	0.3355	0.3355	0.00006
75°	168.55°	0.3835	0.3835	0.00000
90°	180.00°	0.4004	0.4004	0

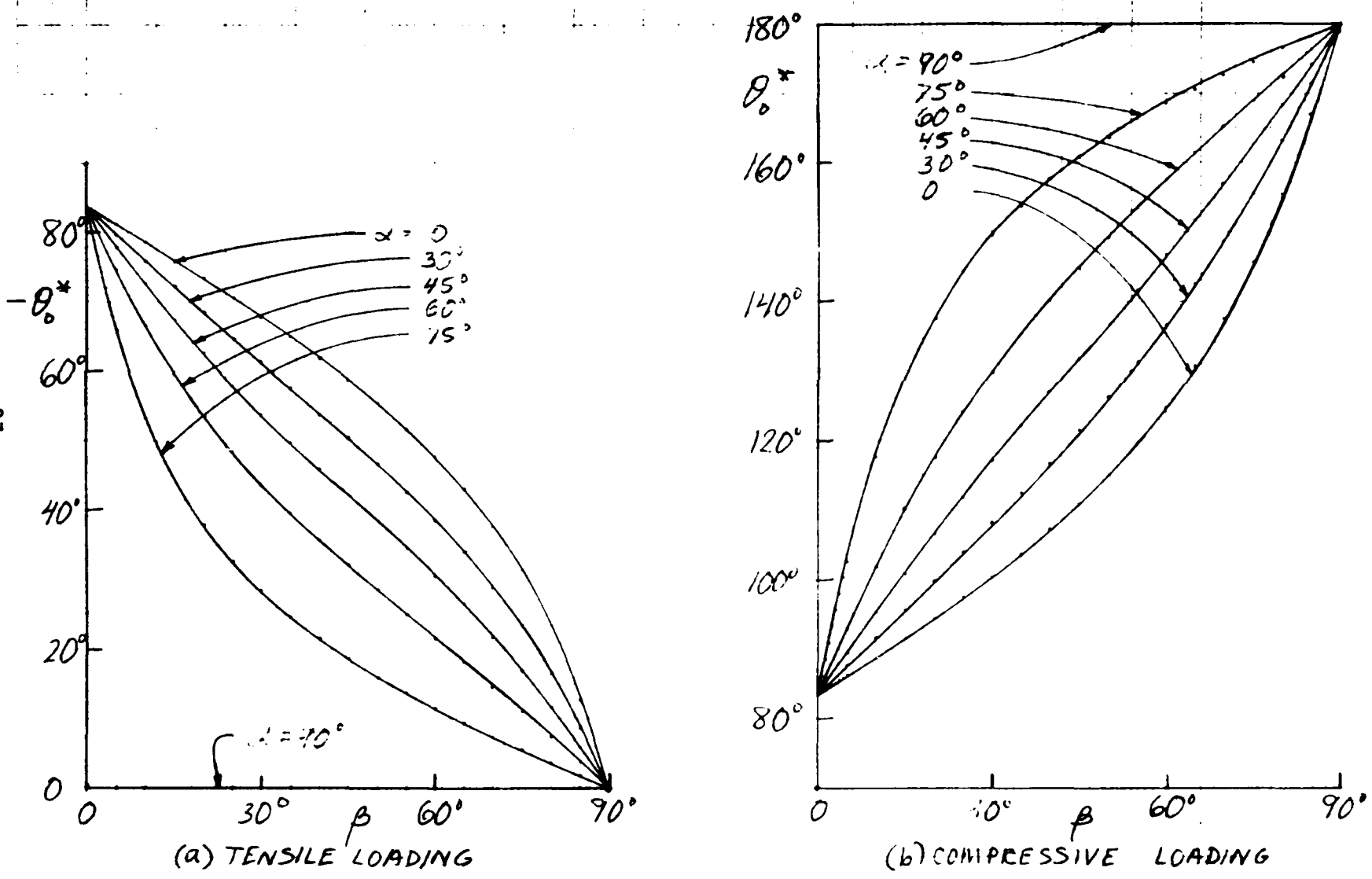

FIG. 6: FRACTURE ANGLES AS FUNCTIONS OF ANGLE OF LOADING FOR VARIOUS POSITIONS AND $b/a = 0.5$, $\nu = 0.33$, $\gamma = 0$.

the load to the plane of the crack. As expected, the fracture angle is zero when the load is perpendicular to the crack ($\beta = 90°$). Figure 6a should be contrasted to Figure 9-4, and 6b to 9-14. The curves in [9] show very different behavior near the ends of the minor axis. Similar statements can be made about Figure 7 in comparison to Figures 9-5 and 9-15. It shows fracture angles for a longer elliptical crack, b/a = 0.1.

Figure 8 shows the influence of the length of the ellipse on fracture angle at the location, $\alpha = 30°$. The longer ellipses approach tunnel cracks (two-dimensional) which for $\omega=0$ are under Mode I and III loading only. As would be expected for this case, the fracture angles approach zero for tensile loading. Again, the curves in Figure 8 are distinctly different from Figures 9-6 and 9-7 for the smaller values of b/a.

Fracture angles for several values of the angle, ω, between the xz-plane and the plane of symmetry of the loading are shown in Figure 9. These angles give the direction in which fracture occurs if it occurs at the ends of the minor axis as is the case for Figures 13 and 14. Figures 9-7 and 9-17 show the same curves as Figure 9 because [9] chose to put ϕ_0 equal to zero, which, to be consistent with other calculations in [9], should have been zero only for $\omega=0$ and 90°. As verified in this Report, the fracture always occurs in the normal plane, and therefore, inadvertently, Figures 9-7 and 9-17 are correct.

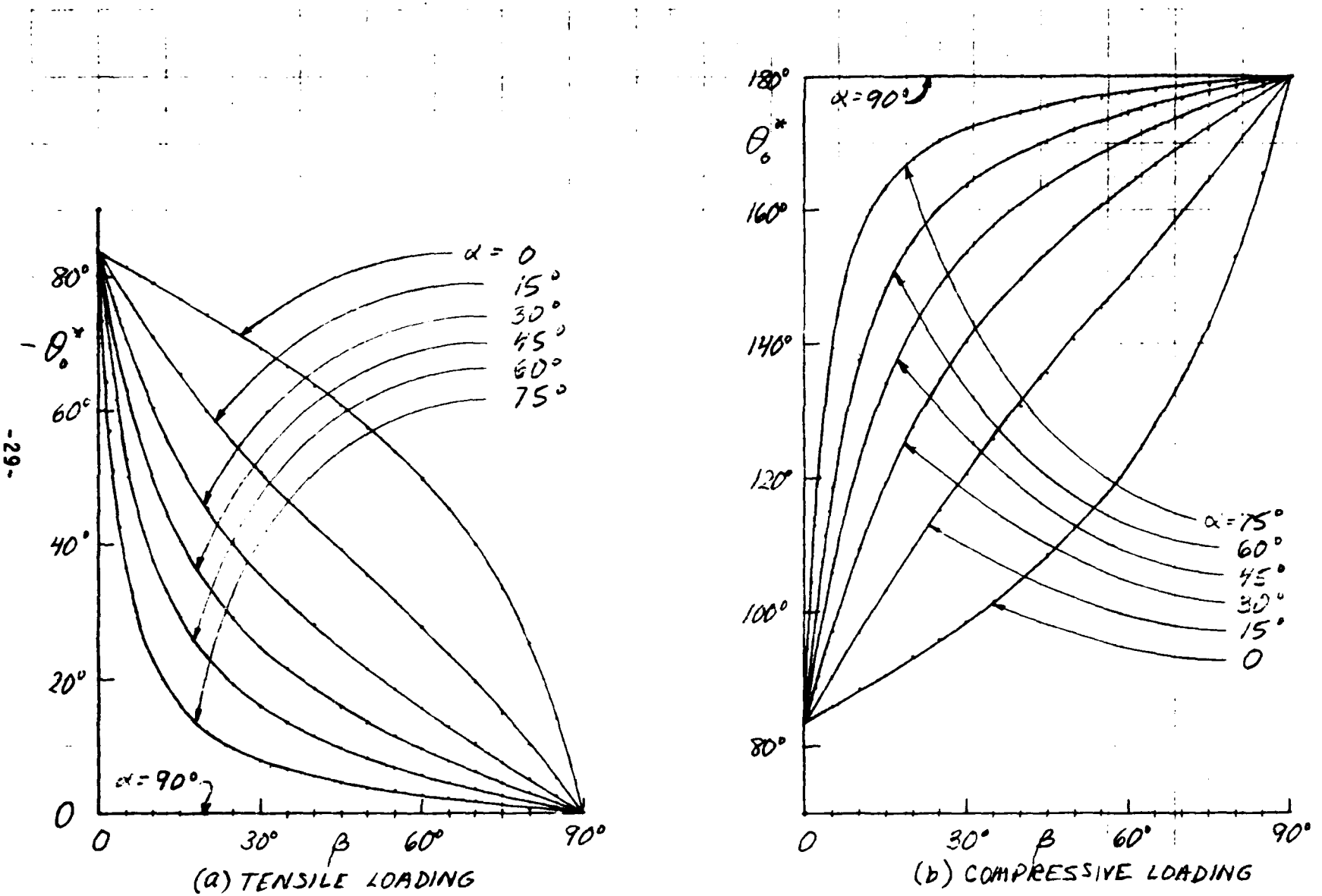

FIG. 7: FRACTURE ANGLES AS FUNCTIONS OF ANGLE OF LOADING FOR VARIOUS POSITIONS AND $b/a = 0.1$, $\nu = 0.33$, $\sigma = 0$.

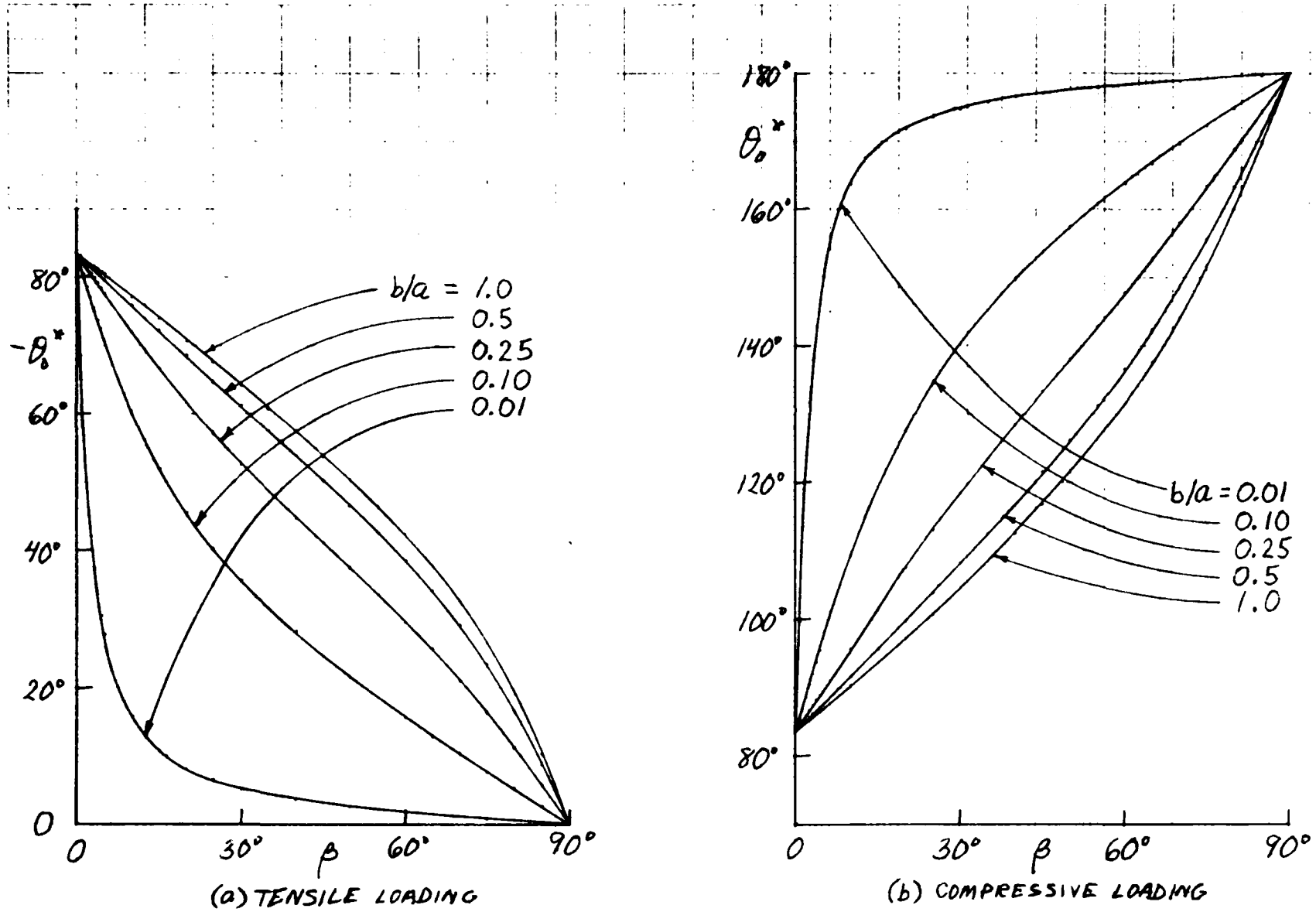

FIG. 8: FRACTURE ANGLES AS FUNCTIONS OF ANGLE OF LOADING FOR VARIOUS CRACK SHAPES AND $\alpha = 30°$, $\nu = 0.33$, $\omega = 0$.

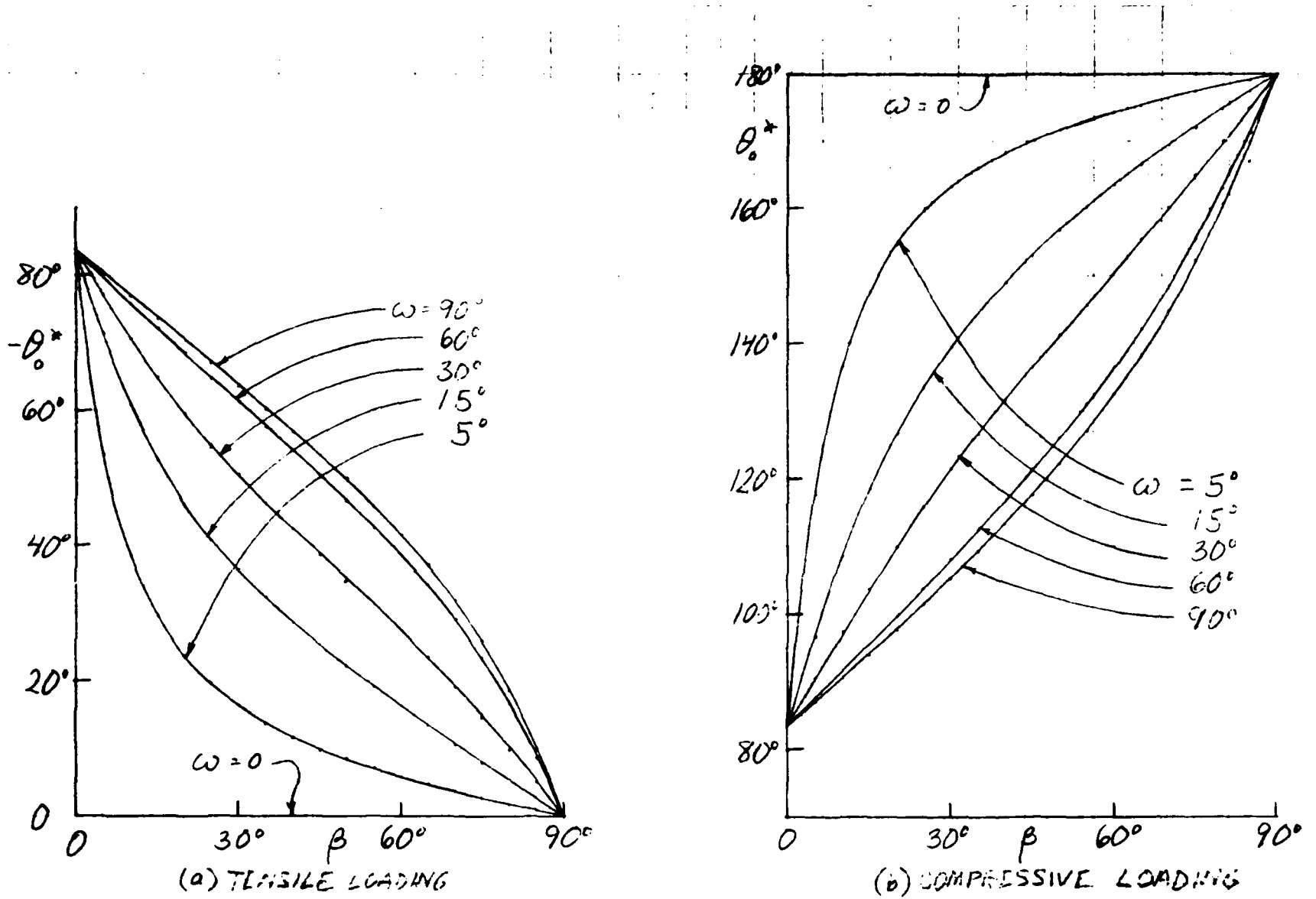

FIG. 9: FRACTURE ANGLES AS FUNCTIONS OF ANGLE OF LOADING FOR VARIOUS PLANES OF LOADING AND $b/a = 0.1$, $\gamma = 0.33$, $\alpha = 70°$

Figures 10, 11, and 12 give the values of minimum strain energy density for various values of the parameters. These curves may be interpreted as giving

$$S^* = F \frac{\sigma^2 b}{16G} \tag{35}$$

where S^* is the minimum strain energy density, and F, as shown in the figures, is a function of α, β, ω, ν, and b/a.

The case of a narrow ellipse (b/a = 0.1) with load applied so that ω=0 is shown in Figure 10. The curves in Figure 9-8 and 9-18 are qualitatively similar, but, except for α=0 and 90°, there are large differences. The case of tensile loading shows peaks for $\beta \approx 55°$. This indicates that failure is more likely to occur when the crack and load make this angle than when they are perpendicular. This type of result, already pointed out in [8,9], requires rethinking of conventional design procedures which consider the worst case to be the one for β = 90°. Compressive loading produces peak values of S^* at $\beta \approx 45°$ and zero values at β=0 and 90°. This implies that extremely large loads (which would cause general yielding and/or crushing) would be required to cause failure in the latter two cases.

Figure 11 shows the effect of b/a on S^*. For nearly circular cracks, there is no peak under tension until β = 90°. Therefore, penny-shaped cracks are in the most detrimental position when normal to the load. When the loads are compressive,

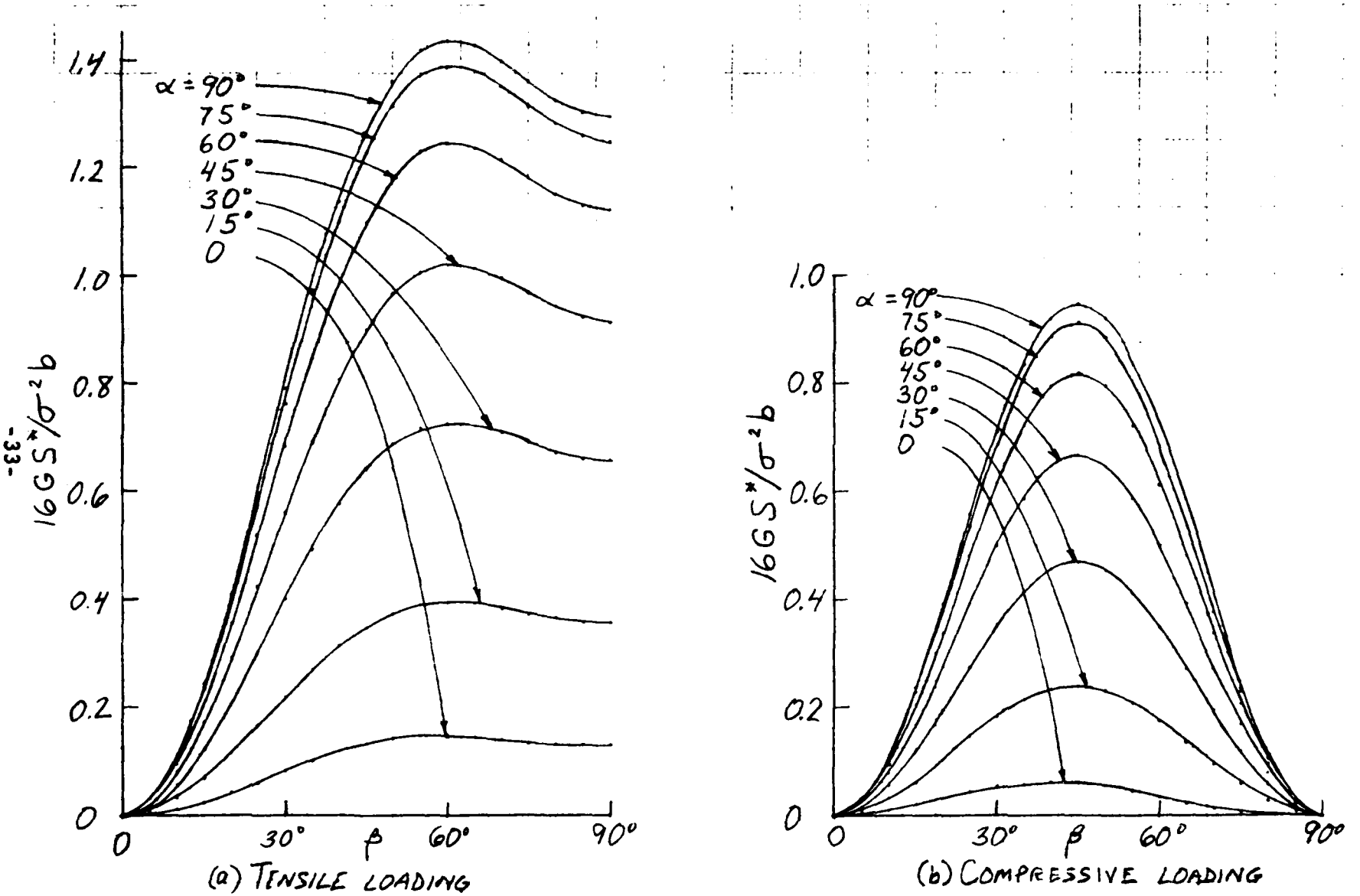

FIG. 10: MINIMUM VALUES OF S ($S^* = S(\theta_0^*)$) AS FUNCTIONS OF ANGLE OF LOADING FOR VARIOUS POSITIONS AND $D/2 = 0.1$, $\nu = 0.33$, $D = 0$.

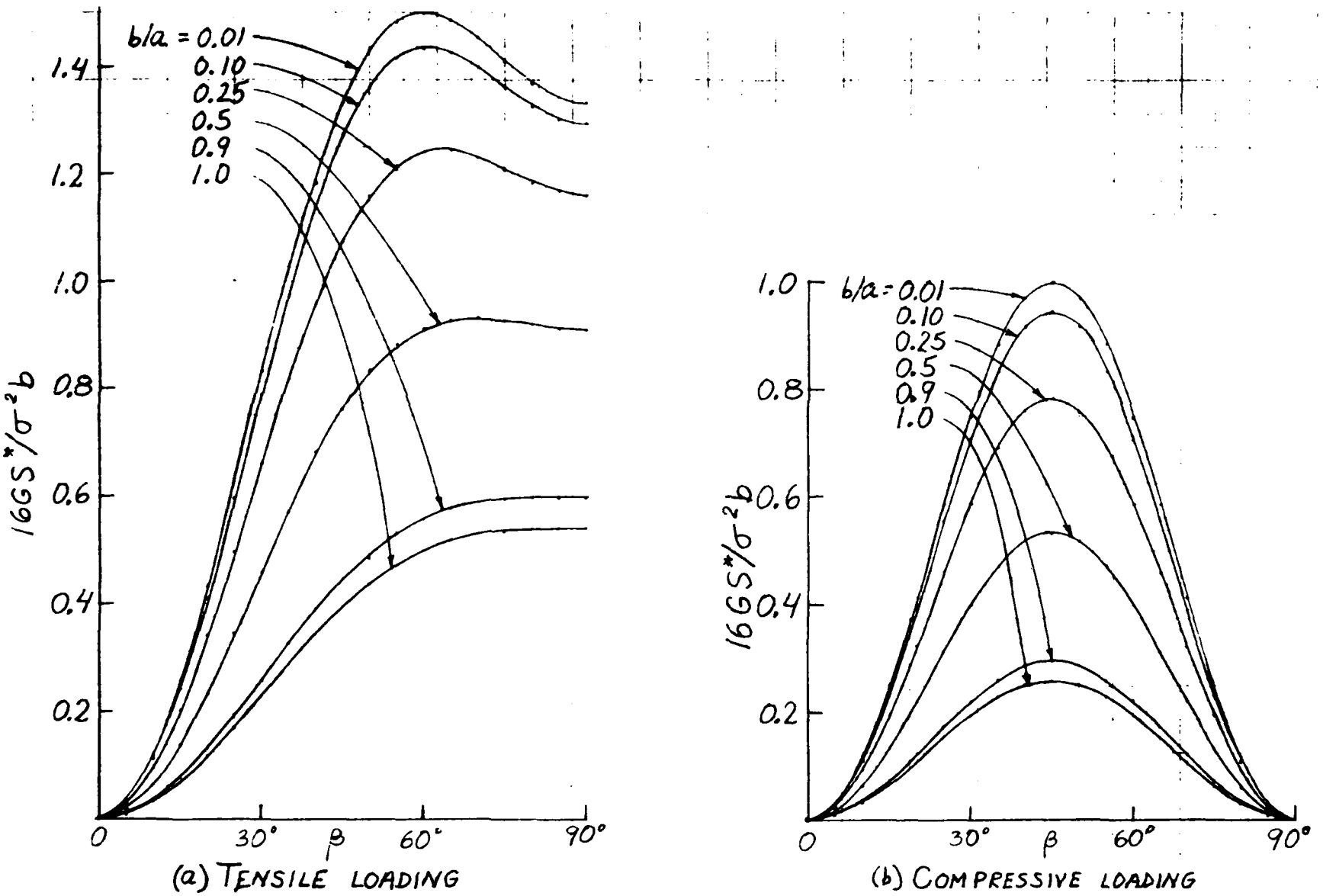

FIG. 11: MINIMUM VALUES OF S ($S^* = S(\theta_0^*)$) AS FUNCTIONS OF ANGLE OF LOADING FOR VARIOUS CRACK SHAPES AND $\alpha = 90°$, $\nu = 0.33$, $\omega = 0$.

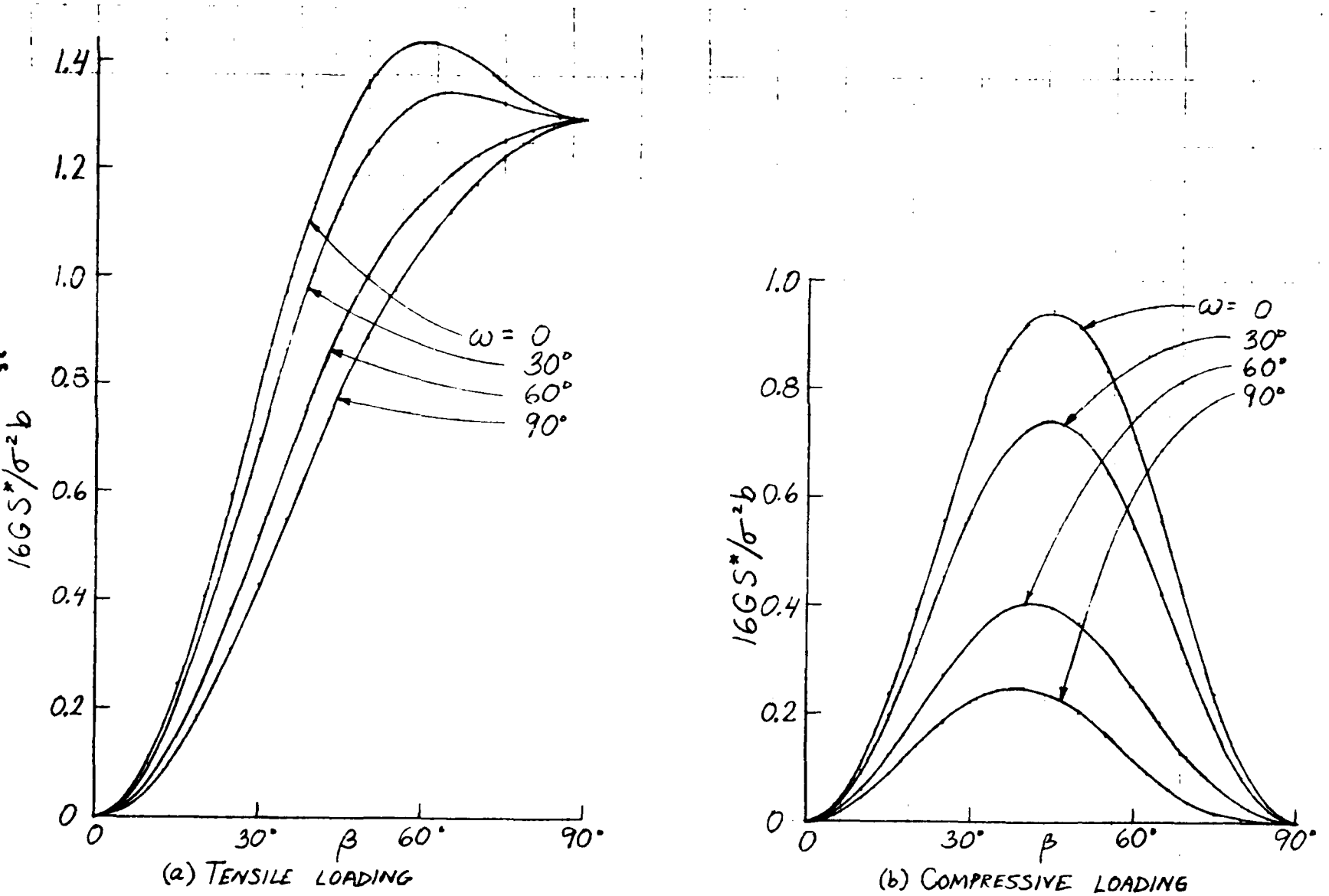

FIG. 12: MINIMUM VALUES OF S ($S^* = S(\theta_0^*)$) AS FUNCTIONS OF ANGLE OF LOADING FOR VARIOUS PLANES OF LOADING AND $b/a = 0.1$, $\nu = 0.33$, $\alpha = 90°$

the peaks are exactly at $\beta = 45°$, and the curves are symmetric about $\beta = 45°$ because at $\alpha = 90°$, only Mode I and III loading are present when $\omega=0$. Figures 9-9 and 9-19 are identical to Figure 11 because of this symmetry.

As discussed in connection with Figure 9, Figures 9-10 and 9-20 are the same as Figure 12 because of an inconsistency in [9] which inadvertently led to the correct result. Figure 12 shows values of S^* at $\alpha = 90°$ for a long ellipse ($b/a = 0.1$) and several orientations of the load. The curve for $\omega=0$ is associated with Mode I and III only, while $\omega = 90°$ produces Mode I and II only at $\alpha = 90°$. For intermediate values of ω, there is a mixture of all three modes of crack deformation. The curves show a decrease in S^* as the load changes from a mixture of Modes I and III to one of Modes I and II.

Failure loads can be obtained from Figures 10, 11, and 12 by applying equations (35) and (25). Solving for the failure load, σ_{cr}, gives

$$\sigma_{cr} = \left[\frac{16GS_{cr}}{bF}\right]^{1/2} \tag{36}$$

or

$$\sigma_{cr} = k_{1c}\left[\frac{4(1-2\nu)}{bF}\right]^{1/2} \tag{37}$$

where F is the function of α, β, ω, ν, and b/a shown in Figures 10, 11, and 12. The form used in equation (37) was chosen

for plotting Figures 13 and 14.

Figure 13 is obtained from Figure 11 with one exception. For most cases, it was found that the largest value of S^* occurs at $\alpha = 90°$. However, for nearly penny-shaped cracks, it sometimes occurs at $\alpha=0$ instead. Therefore, the case of tensile loading shows two curves for $b/a = 1.0$. The upper, solid curve shows the load required to cause failure at $\alpha = 90°$, and the lower, dashed curve gives the load at which failure actually occurs (at $\alpha=0$). It is only in the intermediate range of β that the dashed curve is lower, and so it is not shown outside this range. In all other cases plotted in Figure 13, the failure occurs at $\alpha = 90°$ at the load shown. It is difficult to compare Figures 9-12 and 9-22 with Figure 13, but, by symmetry, they should give the same result. Note that the ordinates in [9] are $2/\pi$ times those in Figures 13 and 14.

Failure loads for the various mixtures of the three modes of crack deformation are shown in Figure 14. This was obtained from Figure 12 by using equation (37). In all cases, the failure occurs at $\alpha = 90°$ for this long elliptical crack ($b/a = 0.1$). It can be verified from Figure 10 that for $\omega=0$ the largest value of S^* occurs at $\alpha = 90°$.

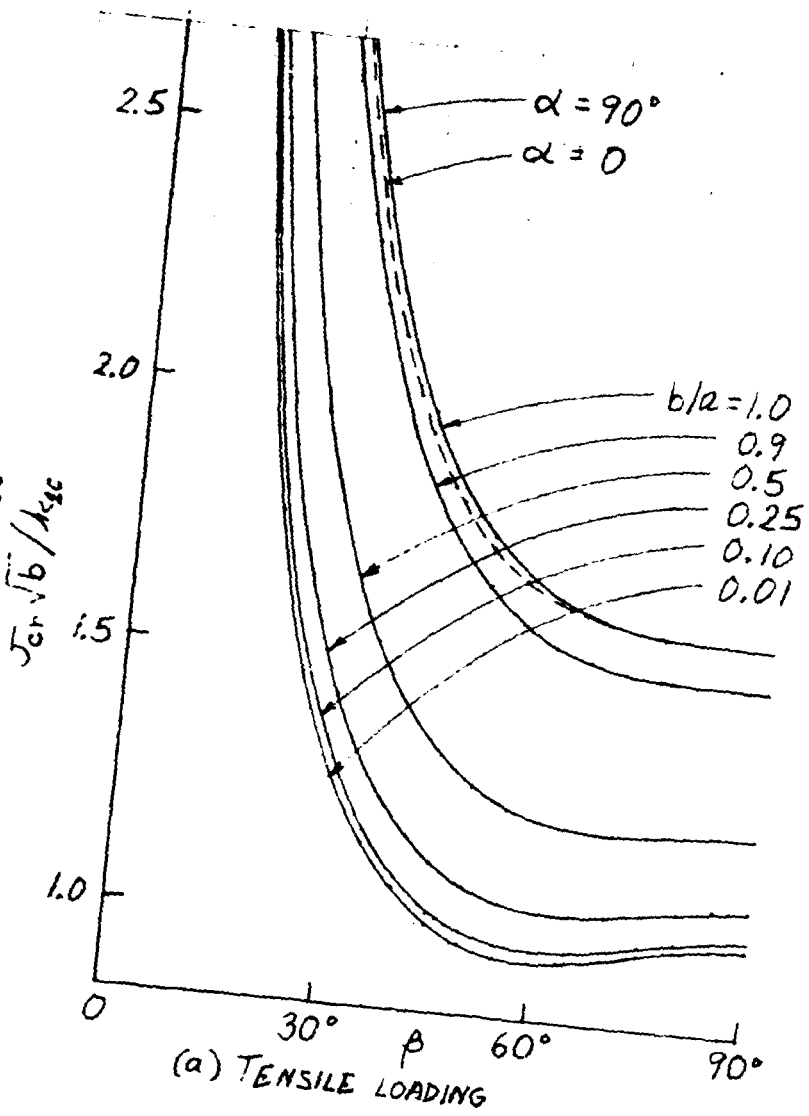

(a) TENSILE LOADING

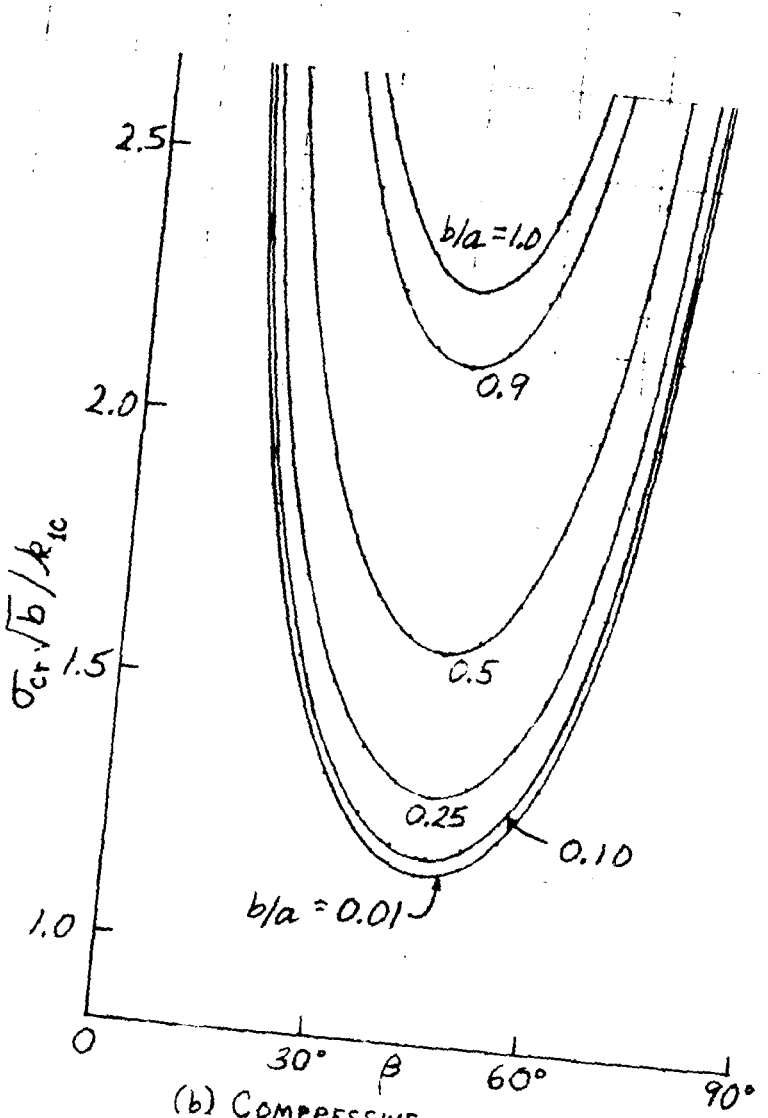

(b) COMPRESSIVE LOADING

FIG. 13: CRITICAL LOADS (FAILURE OCCURS AT $\alpha = 90°$ EXCEPT FOR DASHED CURVE) AS FUNCTIONS OF ANGLE OF LOADING FOR VARIOUS CRACK SHAPES AND $\nu = 0.33$

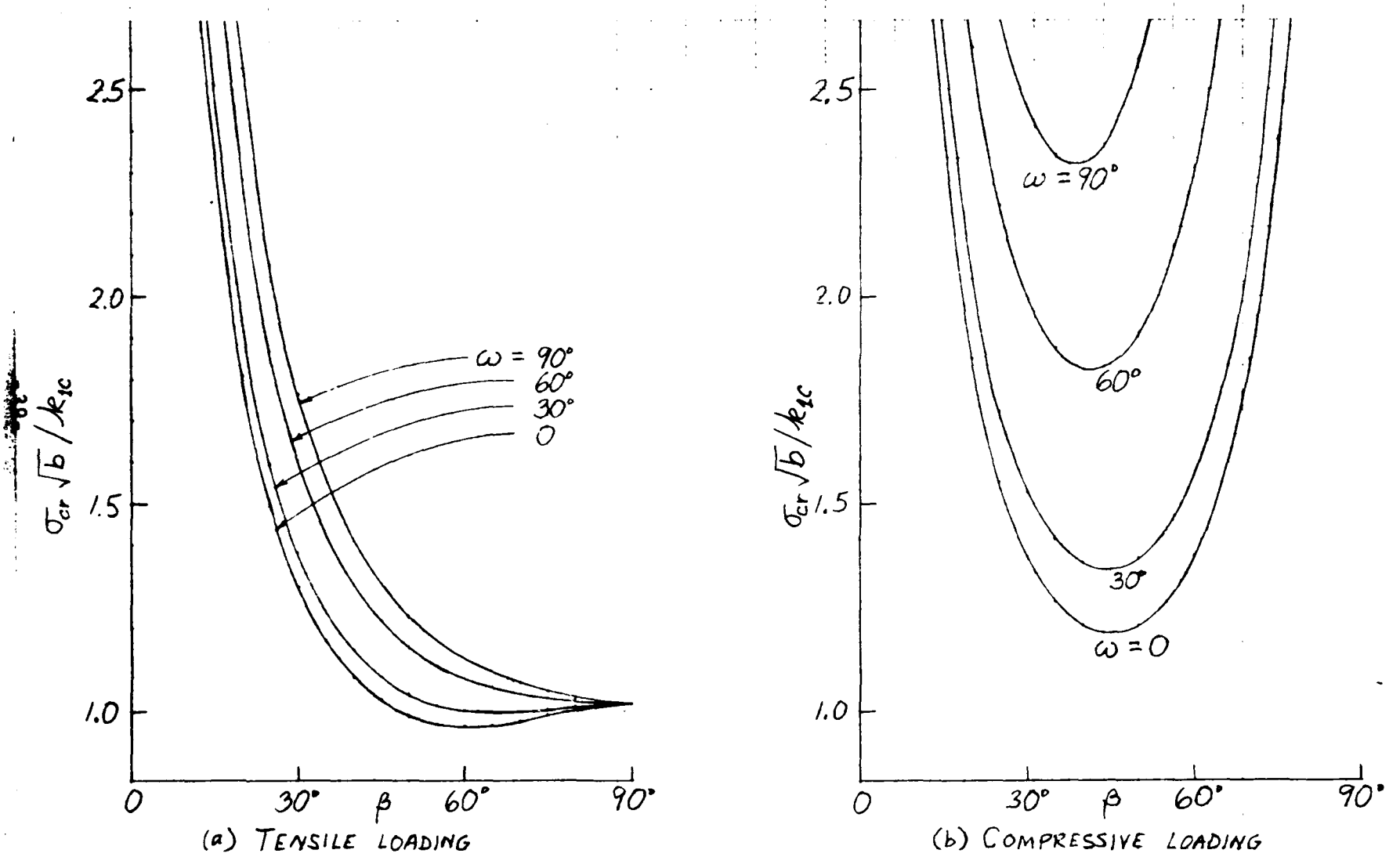

FIG. 14: CRITICAL LOADS (FAILURE OCCURS AT $\alpha = 90°$) AS FUNCTIONS OF ANGLE OF LOADING FOR VARIOUS PLANES OF LOADING AND $b/2 = 0.1$, $\nu = 0.33$.

REFERENCES

1. M. L. Williams, "On the stress distribution at the base of a stationary crack", Journal of Applied Mechanics, Vol. 24, pp. 109-114, 1957.

2. G. C. Sih, "Stress distribution near internal crack tips for longitudinal shear problems", Journal of Applied Mechanics, Vol. 32, pp. 51-58, 1965.

3. R. J. Hartranft and G. C. Sih, "The use of eigenfunction expansions in the general solution of three-dimensional crack problems", Journal of Mathematics and Mechanics, Vol. 19, pp. 123-138, 1969.

4. G. R. Irwin, "Analysis of stresses and strains near the end of a crack traversing a plate", Journal of Applied Mechanics, Vol. 24, pp. 361-364, 1957.

5. I. N. Sneddon, "The distribution of stress in the neighborhood of a crack in an elastic solid", Proceedings of the Royal Society of London, Series A, Vol. 187, pp. 229-260, 1946.

6. M. K. Kassir and G. C. Sih, Three-Dimensional Crack Problems, Noordhoff International Publishing, Leyden, 1975.

7. M. K. Kassir and G. C. Sih, "Three-dimensional stress distribution around an elliptical crack under arbitrary loadings", Journal of Applied Mechanics, Vol. 33, pp. 601-611, 1966.

8. G. C. Sih, "A special theory of crack propagation", Methods of Analysis and Solutions of Crack Problems, pp. XXI-XLV, G. C. Sih, editor, Noordhoff International Publishing, Leyden, 1973.

9. G. C. Sih and B. C. K. Cha, "A fracture criterion for three-dimensional crack problems", Engineering Fracture Mechanics, Vol. 6, pp. 699-723, 1974.

10. G. A. Korn and T. M. Korn, Mathematical Handbook for Scientists and Engineers, pp. 561-584, McGraw-Hill, 1968.

11. M. E. Kipp and G. C. Sih, "The strain energy density failure criterion applied to notched elastic solids", International Journal of Solids and Structures, Vol. 11, pp. 153-173, 1975.

12. R. J. Hartranft and G. C. Sih, "Three-dimensional growth characteristics of a plane crack subjected to concentrated forces", Journal of Applied Mechanics, Vol. 41, pp. 808-809, 1974.

DISTRIBUTION LIST

PART I - GOVERNMENT

Administrative and Liaison Activities

Chief of Naval Research
Department of the Navy
Arlington, Virginia 22217
Attn: Code 439 (3)
461
444

Director
ONR Branch Office
495 Summer Street
Boston, Massachusetts 02210

Director
ONR Branch Office
536 South Clark Street
Chicago, Illinois 60605

Director
Naval Research Laboratory
Attn: Library, Code 2029 (ONRL)
Washington, D.C. 20390 (6)

U.S. Naval Research Laboratory
Attn: Technical Information Division
Washington, D.C. 20390 (6)

Commanding Officer
ONR Branch Office
207 West 24th Street
New York, New York 10011

Director
ONR Branch Office
1030 E. Green Street
Pasadena, California 91101

Defense Documentation Center
Cameron Station
Alexandria, Virginia 22314 (12)

Navy

Chief of Naval Operations
Department of the Navy
Washington, D.C. 20305
Attn: NOP-05F
NOP-506N
NOP-098T

Headquarters
U.S. Marine Corps
Washington, D.C. 20380
Attn: MC-AX-2 (2)
MC-AX-4E2
MC-AAP-3

Commander
Naval Air Systems Command
Department of the Navy
Washington, D.C. 20360
Attn: NAVAIR-320N
NAVAIR-5302
NAVAIR-531
NAVAIR-5311J
NAVAIR-5314
NAVAIR-5325A

Commander
Naval Air Development Center
Warminster, Pennsylvania 18974
Attn: Mr. M. Schulman
Crew Systems Department

Naval Air Development Center
Philadelphia, Pennsylvania 19112
Attn: Dr. E. Hendler
Crew Systems Department

Director
Naval Research Laboratory
Washington, D.C. 20390
Attn: Code 8440 (Dr. F. Rosenthal)

Commanding Officer
Naval Ship Research and Development Center
Bethesda, Maryland 20034
Attn: Code 745 (Mr. B. Whang)

Commanding Officer
Naval Civil Engineering Laboratory
Port Hueneme, California 93041
Attn: Dr. Warren Shaw, Structures Department

Commander
Naval Safety Center
Naval Air Station
Norfolk, Virginia 23511

Capt. Channing L. Ewing Mclusn
Naval Aerospace Medical Research Laboratory
Michoud Assembly Facility
New Orleans, Louisiana 70129

Army

Commanding Officer
U.S. Army Aviation Material Laboratories
Fort Eustis, Virginia 23604
Attn: VDLEU-SS
(Mr. G. T. Singley, III)

Director
U.S. Army Board for Aviation Accident Research
Fort Rucker, Alabama 36360
Attn: BAAR-PP (Mr. J. Haley)

Commanding Officer
U.S. Army Research Office Durham
Attn: Mr. J. J. Murray
CRD-AA-IP
Box CM, Duke Station
Durham, North Carolina 27706

Air Force

Air Force Office of Scientific Research
1400 Wilson Boulevard
Arlington, Virginia 22209
Attn: Mechs. Div.

Commanding Officer
6571st AMRL
Holloman Air Force Base, New Mexico
Attn: Mr. C. C. Gragg

NASA

Mr. C. Kubokawa
N239-3
NASA Ames Research Center
Moffett Field, California 94035

Department of Transportation

Mr. R. F. Chandler
Code AC 119
CAMI, FAA Aeronautical Center
P.O. Box 25082
Oklahoma City, Oklahoma 73123

Mr. H. Spicer
Federal Aviation Administration (DS-41)
800 Independence Avenue, S.W.
Washington, D.C. 20590

Mr. H. Daiutolo
Federal Aviation Administration
NAFEC (NA541)
Atlantic City, New Jersey 08405

Mr. D. Beyer
Federal Aviation Administration (RD-730)
800 Independence Avenue, S.W.
Washington, D.C. 20590

Headquarters
U.S. Coast Guard
400 7th Street, S.W.
Washington, D.C. 20590
Attn: DAT/62
EAE/63
ENE-5/64
IGS-1/61
NMT-t/82
OSR-2/73

Mr. J. G. Viner
Protective Systems Group (RS-12)
Federal Highway Administration
400 7th Street, S.W.
Washington, D.C. 20590

Mr. W. H. Collins
Computer Technology Group (DV-11)
Federal Highway Administration
400 7th Street, S.W.
Washington, D.C. 20590

Mr. Kenneth Batcheller, Chief
Safety Programs Division (RS-20)
Federal Railroad Administration
400 7th Street, S.W.
Washington, D.C. 20590

Mr. E. Ward, Chief
Engineering Research and Development Division (RT-20)
Federal Railroad Administration
400 7th Street, S.W.
Washington, D.C. 20590

Dr. J. A. Edwards
Associate Administrator for Research and Development
National Highway Traffic Safety Administration
400 7th Street, S.W.
Washington, D.C. 20590

Mr. C. D. Ferguson
Office of Crashworthiness (41-40)
National Highway Traffic Safety Administration
400 7th Street, S.W.
Washington, D.C. 20590

Mr. L. L. Bradford
Office of Vehicle Structures Research (43-50)
National Highway Traffic Safety Administration
400 7th Street, S.W.
Washington, D.C. 20590

National Transportation Safety Board
800 Independence Avenue, S.W.
Washington, D.C. 20590
Attn: Mr. A. L. Schmieg, NS-10
Mr. H. L. Morgan, NS-20
Mr. B. C. Doyle, NA-87

Dr. H. E. vonGierke
Aerospace Medical Research Laboratory
Aerospace Medical Division
Air Force Systems Command
Wright-Patterson Air Force Base, Ohio 45433

Sal Davis
Fairchild Industries, Inc.
Fairchild Republic Division
Farmingdale, New York 11735

Part II - CONTRACTORS AND OTHER TECHNICAL COLLABORATORS

Mr. S. P. Desjardins
Dynamic Science
1800 West Deer Valley Drive
Phoenix, Arizona 85027

Dr. A. A. Ezra, Chairman
Department of Mechanical Sciences and Environmental Engineering
University of Denver
Denver, Colorado 80210

Dr. Albert I. King
Bioengineering Center
Wayne State University
Detroit, Michigan 48202

Dr. R. C. DeHart, Director
Department of Structural Research
Southwest Research Institute
P.O. Drawer 28510
San Antonio, Texas 78284

Professor J. B. Martin
Division of Engineering
Brown University
Providence, Rhode Island 02912

Dr. J. L. Tocher
Boeing Computer Services (72-80)
P.O. Box 24346
Seattle, Washington 98124

Mr. D. G. Harding, Manager
Survivability Staff
Boeing Company - Vertol Division
Philadelphia, Pennsylvania 19142

Dr. H. E. Lindberg, Manager
Engineering Mechanics Program
Stanford Research Institute
Menlo Park, California 94025

Mr. John W. Freyler
Beta Industries, Inc.
2763 Culver Avenue
Dayton, Ohio 45429

Dr. L. E. Hulbert, Chief
Advanced Solid Mechanics Division
505 King Avenue
Columbus, Ohio 43201

Professor George Sih
Department of Mechanics
Lehigh University
Bethlehem, Pennsylvania 18015

Dr. Harold Liebowitz, Dean
School of Engineering and
Applied Science
George Washington University
725 23rd Street
Washington, D.C. 20006

Professor S. B. Dong
University of California
Department of Mechanics
Los Angeles, California 90024

Professor A. J. Durelli
Mechanics Division
The Catholic University of
America
Washington, D.C. 20017

Professor H. H. Bleich
Department of Civil Engineering
Columbia University
Amsterdam & 120th Street
New York, New York 10027

Professor A. M. Freudenthal
George Washington University
School of Engineering and
Applied Science
Washington, D.C. 20006

Professor P. G. Hodge
Department of Mechanics
Illinois Institute of Technology
Chicago, Illinois 60616

Professor D. C. Drucker
Dean of Engineering
University of Illinois
Urbana, Illinois 61801

Professor N. M. Newmark
Department of Civil Engineering
University of Illinois
Urbana, Illinois 61801

Library (Code 0384)
U.S. Naval Postgraduate School
Monterey, California 93940

Dr. Francis Cozzarelli
Division of Interdisciplinary Studies
and Research
School of Engineering
State University of New York
Buffalo, New York 14214

Dr. George Herrmann
Stanford University
Department of Applied Mechanics
Stanford, California 94305

Professor J. D. Achenbach
Technological Institute
Northwestern University
Evanston, Illinois 60201

Professor J. Kempner
Department of Aero. Engrg. and
Applied Mech.
Polytechnic Institute of Brooklyn
333 Jay Street
Brooklyn, New York 11201

Dr. Nicholas J. Hoff
Dept. of Aero. and Astro.
Stanford University
Stanford, California 94305

Professor Norman Jones
Massachusetts Institute of Tech-
nology
Department of Naval Architecture
and Marine Engineering
Cambridge, Massachusetts 02139

Professor Werner Goldsmith
Department of Mechanical
Engineering
Division of Applied Mechanics
University of California
Berkeley, California 94720

Professor W. D. Pilkey
Department of Aerospace Engineering
University of Virginia
Charlottesville, Virginia 22903

Dr. H. N. Abramson
Southwest Research Institute
8500 Culebra Road
San Antonio, Texas 78206

Mr. John Scowcroft
Automobile Manufactures Association
330 New Center Building
Detroit, Michigan 48202

Dr. R. D. Young
Texas Transportation Institute
Texas A & M University
College Station, Texas 77840

Professor J. A. Collins
Mechanical Engineering Department
Arizona State University
Tempe, Arizona 85281

Unclassified

SECURITY CLASSIFICATION OF THIS PAGE *(When Data Entered)*

REPORT DOCUMENTATION PAGE	READ INSTRUCTIONS BEFORE COMPLETING FORM
1. REPORT NUMBER: IFSM-76-74 (14)	2. GOVT ACCESSION NO.
3. RECIPIENT'S CATALOG NUMBER	
4. TITLE *(and Subtitle)*: Stress Singularity for a Crack with an Arbitrarily Curved Front. (6)	5. TYPE OF REPORT & PERIOD COVERED: Technical Report. (9)
6. PERFORMING ORG. REPORT NUMBER	
7. AUTHOR(s): R. J. Hartranft, G. C. Sih (10)	8. CONTRACT OR GRANT NUMBER(s): N00014-76-C-0094 (15) NEW
9. PERFORMING ORGANIZATION NAME AND ADDRESS: Lehigh University, Institute of Fracture & Solid Mechanics, Bethlehem, Pennsylvania 18015	10. PROGRAM ELEMENT, PROJECT, TASK AREA & WORK UNIT NUMBERS: N00014-76-C-0094
11. CONTROLLING OFFICE NAME AND ADDRESS: Department of the Navy, Office of Naval Research, Arlington, Virginia 22217 (11)	12. REPORT DATE: April 1976
	13. NUMBER OF PAGES: 43
14. MONITORING AGENCY NAME & ADDRESS *(if different from Controlling Office)* (12) 45 p.	15. SECURITY CLASS. *(of this report)*
	15a. DECLASSIFICATION/DOWNGRADING SCHEDULE

16. DISTRIBUTION STATEMENT *(of this Report)*

Approved for public release; distribution unlimited.

17. DISTRIBUTION STATEMENT *(of the abstract entered in Block 20, if different from Report)*

18. SUPPLEMENTARY NOTES

19. KEY WORDS *(Continue on reverse side if necessary and identify by block number)*

strain energy density
crack front stress field
crack path
three-dimensional analysis

20. ABSTRACT *(Continue on reverse side if necessary and identify by block number)*

To investigate the possibility of a point of a crack front propagating in a direction not in the normal plane of the crack front, the three-dimensional form of the crack front stress field is obtained. To simplify comparisons of the states of stress at various points lying on a spherical surface centered at a point of the crack front, a local spherical coordinate system is used. It is found that the crack propagation will be from each point of the

DD FORM 1 JAN 73 1473 EDITION OF 1 NOV 65 IS OBSOLETE

407 099

Unclassified

SECURITY CLASSIFICATION OF THIS PAGE *(When Data Entered)*

crack front in a direction lying in the normal plane.

The results are used in conjunction with the strain energy density fracture criterion for the problem of an elliptical crack. The plane of the flat elliptical crack makes an arbitrary angle with the field of uniform applied tensile stress. Crack growth directions for various positions along the crack front are determined, and loads required for fracture for various angles are obtained.

INSTRUCTIONS FOR PREPARATION OF REPORT DOCUMENTATION PAGE

RESPONSIBILITY. The controlling DoD office will be responsible for completion of the Report Documentation Page, DD Form 1473, in all technical reports prepared by or for DoD organizations.

CLASSIFICATION. Since this Report Documentation Page, DD Form 1473, is used in preparing announcements, bibliographies, and data banks, it should be unclassified if possible. If a classification is required, identify the classified items on the page by the appropriate symbol.

COMPLETION GUIDE

General. Make Blocks 1, 4, 5, 6, 7, 11, 13, 15, and 16 agree with the corresponding information on the report cover. Leave Blocks 2 and 3 blank.

Block 1. Report Number. Enter the unique alphanumeric report number shown on the cover.

Block 2. Government Accession No. Leave Blank. This space is for use by the Defense Documentation Center.

Block 3. *Recipient's Catalog Number.* Leave blank. This space is for the use of the report recipient to assist in future retrieval of the document.

Block 4. Title and Subtitle. Enter the title in all capital letters exactly as it appears on the publication. Titles should be unclassified whenever possible. Write out the English equivalent for Greek letters and mathematical symbols in the title (see *"Abstracting Scientific and Technical Reports of Defense-sponsored RDT&E," AD-667 000).* If the report has a subtitle, this subtitle should follow the main title, be separated by a comma or semicolon if appropriate, and be initially capitalized. If a publication has a title in a foreign language, translate the title into English and follow the English translation with the title in the original language. Make every effort to simplify the title before publication.

Block 5. Type of Report and Period Covered. Indicate here whether report is interim, final, etc., and, if applicable, inclusive dates of period covered, such as the life of a contract covered in a final contractor report.

Block 6. Performing Organization Report Number. Only numbers other than the official report number shown in Block 1, such as series numbers for in-house reports or a contractor, grantee number assigned by him, will be placed in this space. If no such numbers are used, leave this space blank.

Block 7. Author(s). Include corresponding information from the report cover. Give the name(s) of the author(s) in conventional order (for example, John R. Doe or, if author prefers, J. Robert Doe). In addition, list the affiliation of an author if it differs from that of the performing organization.

Block 8. Contract or Grant Number(s). For a contractor or grantee report, enter the complete contract or grant number(s) under which the work reported was accomplished. Leave blank in in-house reports.

Block 9. Performing Organization Name and Address. For in-house reports enter the name and address, including office symbol, of the performing activity. For contractor or grantee reports enter the name and address of the contractor or grantee who prepared the report and identify the appropriate corporate division, school, laboratory, etc., of the author. List city, state, and ZIP Code.

Block 10. Program Element, Project, Task Area, and Work Unit Numbers. Enter here the number code from the applicable Department of Defense form, such as the DD Form 1498, "Research and Technology Work Unit Summary" or the DD Form 1634 "Research and Development Planning Summary," which identifies the program element, project, task area, and work unit or equivalent under which the work was authorized.

Block 11. Controlling Office Name and Address. Enter the full, official name and address, including office symbol, of the controlling office. (Equates to funding/sponsoring agency. For definition see DoD Directive 5200.20, "Distribution Statements on Technical Documents.")

Block 12. Report Date. Enter here the day, month, and year or month and year as shown on the cover.

Block 13. Number of Pages. Enter the total number of pages.

Block 14. Monitoring Agency Name and Address (if different from Controlling Office). For use when the controlling or funding office does not directly administer a project, contract, or grant, but delegates the administrative responsibility to another organization.

Blocks 15 & 15a. Security Classification of the Report: Declassification/Downgrading Schedule of the Report. Enter in 15 the highest classification of the report. If appropriate, enter in 15a the declassification/downgrading schedule of the report, using the abbreviations for declassification/downgrading schedules listed in paragraph 4-207 of DoD 5200.1-R.

Block 16. Distribution Statement of the Report. Insert here the applicable distribution statement of the report from DoD Directive 5200.20, "Distribution Statements on Technical Documents."

Block 17. Distribution Statement (of the abstract entered in Block 20, if different from the distribution statement of the report). Insert here the applicable distribution statement of the abstract from DoD Directive 5200.20, "Distribution Statements on Technical Documents."

Block 18. Supplementary Notes. Enter information not included elsewhere but useful, such as: Prepared in cooperation with . . . Translation of (or by) . . . Presented at conference of . . . To be published in . . .

Block 19. Key Words. Select terms or short phrases that identify the principal subjects covered in the report, and are sufficiently specific and precise to be used as index entries for cataloging, conforming to standard terminology. The DoD "Thesaurus of Engineering and Scientific Terms" (TEST), AD-672 000, can be helpful.

Block 20. Abstract. The abstract should be a brief (not to exceed 200 words) factual summary of the most significant information contained in the report. If possible, the abstract of a classified report should be unclassified and the abstract to an unclassified report should consist of publicly- releasable information. If the report contains a significant bibliography or literature survey, mention it here. For information on preparing abstracts see "Abstracting Scientific and Technical Reports of Defense-Sponsored RDT&E," AD-667 000.

GPO 860-885